

The role of disordered dynamics on the nature of transition in a turbulent reactive flow system

Sivakumar Sudarsanan,^{1,2} Induja Pavithran,^{1,2} and R. I. Sujith^{1,2}

¹*Department of Aerospace Engineering, Indian Institute of Technology Madras, Chennai 600 036, India*

²*Centre of Excellence for Studying Critical Transition in Complex Systems, Indian Institute of Technology Madras, Chennai 600 036, India*

(*Electronic mail: sujith@iitm.ac.in)

(Dated: 24 September 2024)

The transition from a chaotic to a periodic oscillatory state can be smooth or abrupt in real-world turbulent systems. Although there have been several mathematical studies, the occurrence of abrupt transitions in real-world systems such as turbulent reactive flow systems is not well understood. A turbulent reactive flow system consists of the flame, the acoustic field, and the hydrodynamic field interacting nonlinearly. Generally, as the Reynolds number is increased, a laminar flow becomes turbulent, and the range of time scales associated with the flow broadens. Yet, as the Reynolds number is increased in a turbulent reactive flow system, a single dominant time scale emerges in the acoustic pressure oscillations, indicated by its loss of multifractality. For such smooth and abrupt transitions from chaos to order, we study the evolution of correlated and uncorrelated dynamics between the acoustic pressure and the heat release rate oscillations in the spatiotemporal domain of the turbulent reactive system. The correlated dynamics that add or remove energy from the acoustic field are defined as conformists and contrarians, respectively. The uncorrelated dynamics, neither adds nor removes energy is defined as disorder. Conformist dynamics dominate the contrarian dynamics as order emerges from chaos. We discover that the spatial extent of the disordered dynamics plays a critical role in deciding the nature of the transition. During the smooth transition, we observe a significant presence of disordered dynamics in the spatial domain. In contrast, abrupt transitions are accompanied by the disappearance of disordered dynamics from the spatial domain.

I. INTRODUCTION

The emergence of periodic oscillations or order from a state of chaos is intriguing; this transition can occur in a smooth or abrupt manner¹⁻⁴. The amplitude of these periodic oscillations gradually increases during smooth, continuous phase transitions from chaos to order in far-from-equilibrium turbulent reactive flow systems^{1,2}. In contrast, an abrupt transition from chaos to order is associated with an explosive rise in the amplitude of the periodic oscillations with a hysteresis behavior^{3,4}. Abrupt transitions are more dangerous than smooth transitions. Examples of such abrupt transitions are tipping in climate systems⁵, epileptic seizures⁶, and occurrence of violent high-amplitude periodic acoustic pressure oscillations in aircraft and rocket engines⁴.

Abrupt transitions have been studied from the context of explosive synchronization and explosive percolation transition⁷⁻⁹. Studies using mathematical models suggest that explosive synchronization transition arises in a network of phase oscillators under conditions of uniform frequency distribution of phase oscillators¹⁰, positive correlation between the degree of an oscillator (degree is defined as the number of oscillators connected to a particular oscillator) and its frequency^{11,12}, and higher-order interactions between the phase oscillators^{13,14}. Furthermore, studies show that the negatively coupled oscillators and positively coupled oscillators play a pivotal role in the occurrence of abrupt transition¹⁵⁻¹⁷. Such positive and negative interactions are observed in neuronal^{18,19}, social²⁰, and ecological²¹ systems. In synchronization theory, the positively and negatively coupled oscillators are referred to as conformists and contrarians²². Apart from several studies using mathematical models, only a few experimental studies on abrupt transitions have been reported^{3,4,23-27}. In this paper, we present how smooth and abrupt phase transitions occur in an experimental turbulent reactive flow system (Fig. 1a) that is far from equilibrium.

The turbulent reactive flow system comprises three interconnected subsystems: the flame, the acoustic pressure, and the turbulent, hydrodynamic flow field. In our study, the control parameter, the Reynolds number is defined as the ratio of inertial to the viscous force. In fluid flow systems, as the Reynolds number is increased, a laminar fluid flow becomes turbulent and the range of time scales associated with the flow increases²⁸. In contrast, as the Reynolds number is increased in a turbulent reactive flow system, we observe that the chaotic fluctuations characterized by a multifractal spectrum lose their multifractal nature, and a single dominant time scale (periodic oscillations) emerges in the acoustic pressure²⁹. The emergence of periodic oscillations is due to the positive feedback loop arising from the nonlinear interaction between the subsystems^{30,31}.

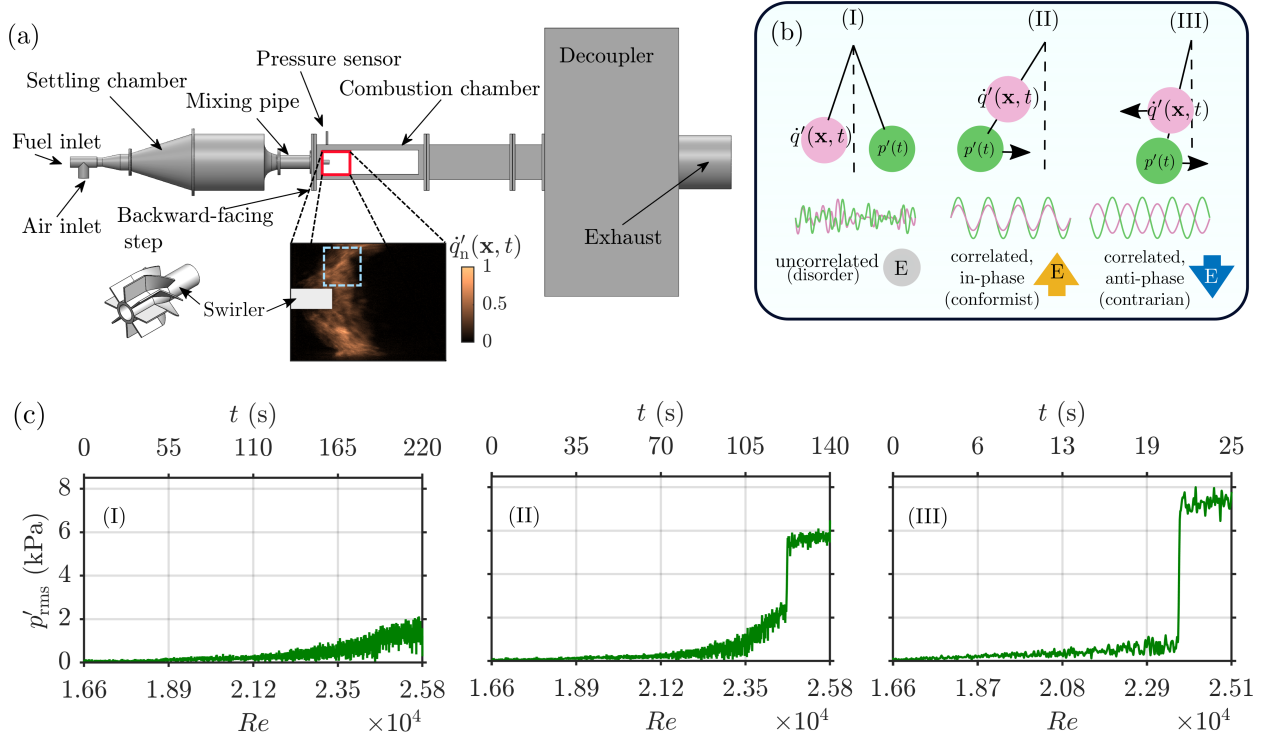


FIG. 1. A schematic of the experimental system consisting of air and fuel inlet ports, a settling chamber, a swirler used for flame stabilization, a combustion chamber, and a decoupler. A piezoelectric pressure transducer attached to the top side of the combustion chamber is used to acquire the acoustic pressure measurements. The heat release rate dynamics (CH* images) were recorded using a high-speed camera. The zoomed-in view of the swirler and the combustion chamber are shown in (a). The region inside the blue dashed rectangle in the inset of (a) is considered for the analysis. (b) We demonstrate the uncorrelated and correlated dynamics using the schematic of two coupled pendulums. The pink and the green pendulums represent the heat release rate ($\dot{q}'(\mathbf{x}, t)$) and the acoustic pressure ($p'(t)$) oscillators. The same direction of the arrow marks for $\dot{q}'(\mathbf{x}, t)$ and $p'(t)$ signifies in-phase oscillations, while the opposite direction indicates anti-phase oscillations. (b-I) The uncorrelated fluctuations neither add nor remove energy from the acoustic pressure field (disordered dynamics). (b-II) If $p'(t)$ and $\dot{q}'(\mathbf{x}, t)$ oscillations are correlated and in-phase ($|\Delta\phi| < \pi/2$), energy will be added to the acoustic field (conformist dynamics). (b-III) If $p'(t)$ and $\dot{q}'(\mathbf{x}, t)$ are correlated and anti-phase ($\pi/2 < |\Delta\phi| < \pi$), energy will be removed from the acoustic field (contrarian dynamics). (c) The evolution of the root-mean-square (rms) values of $p'(t)$ calculated for a moving window of duration 0.5 s corresponding to (I) a smooth transition, (II) a smooth transition followed by an abrupt transition, and (III) an abrupt transition as the Reynolds number is continuously increased for three different experimental conditions.

The self-sustained periodic oscillatory state of large amplitude in turbulent reactive flow systems is known as thermoacoustic instability. Thermoacoustic instability is observed in aircraft engines, rocket engines and land-based gas turbine power plants^{32–34}. The occurrence of such a large amplitude oscillatory state is undesirable, as it can lead to catastrophic system failures^{32–35}.

The transition to the state of thermoacoustic instability in turbulent systems is manifested as

the emergence of order from chaos³⁰. In turbulent systems, the transition from chaos to thermoacoustic instability was observed to be smooth via a state of intermittency characterized by epochs of periodic oscillations amidst aperiodic fluctuations¹. The growth of amplitude of the acoustic pressure oscillations during this transition follows universal scaling relations with fractal and spectral measures of the acoustic pressure oscillations^{36,37}. The presence of intermittency and the observed scaling relations helped in developing early warning measures for impending thermoacoustic instability²⁹. During the state of chaos, small and disconnected patches of ordered regions (spatial locations exhibiting the correlated dynamics between the heat release rate and the acoustic pressure oscillations) are observed in the spatial domain^{2,38}. These small ordered regions merge and form a giant cluster spanning the entire spatial domain during the state of thermoacoustic instability^{2,38}. For a smooth transition, the distribution of the size of the patterns of ordered regions exhibits scaling laws that fall under the universality class of 2+1 directed percolation². Recently, abrupt transitions to a very high amplitude periodic oscillatory state in turbulent reactive flow systems have also been reported^{3,4,39}. Such an abrupt switch to a high amplitude state is very dangerous in a practical scenario. Significant studies on smooth transitions in turbulent reactive flow systems have been conducted; however, the occurrence of abrupt transitions in these systems has not been well studied.

In this work, we study the dynamics between the heat release rate and the acoustic pressure oscillations in the spatiotemporal domain of the system during a (1) smooth transition, (2) a smooth transition followed by an abrupt transition, and (3) an abrupt transition, as the Reynolds number is continuously increased for three different experimental conditions (Fig. 1c) (refer to *Materials and Methods* for more details on the experimental conditions). In this regard, first, we discuss the influence of the correlated and uncorrelated dynamics of the heat release rate and the acoustic pressure fluctuations on the acoustic energy of the system.

II. ROLE OF CONFORMIST, CONTRARIAN, AND DISORDERED DYNAMICS

The illustration in Fig. 1b represents the influence of the uncorrelated and correlated dynamics between the heat release rate ($\dot{q}'(\mathbf{x}, t)$) and the acoustic pressure fluctuations ($p'(t)$) on the acoustic energy of the reactive flow systems. The acoustic energy source is characterized by the correlation

between the heat release rate and the acoustic pressure oscillations⁴⁰, which can be expressed as

$$\mathcal{R} = \int_0^T p'(t) \dot{q}'(\mathbf{x}, t) dt. \quad (1)$$

Here, T is the time period of the acoustic pressure oscillations⁴¹. During the uncorrelated dynamics (as shown in Fig. 1b-I), where $\dot{q}'(\mathbf{x}, t)$ and $p'(t)$ are desynchronized and exhibiting aperiodic oscillations, the correlation value (\mathcal{R}) is very minimal, and the energy is neither added nor removed from the acoustic field. Such uncorrelated dynamics signifies the underlying turbulent nature of the fluid flow. During the correlated dynamics as shown in Fig. 1b-II and Fig. 1b-III, energy is either added to or removed from the acoustic field depending upon the phase difference ($\Delta\phi$) between $\dot{q}'(\mathbf{x}, t)$ and $p'(t)$. If $\dot{q}'(\mathbf{x}, t)$ and $p'(t)$ are in-phase ($|\Delta\phi| < \pi/2$), energy is added locally to the acoustic field (Fig. 1b-II)^{40,42}. On the other hand, if $\dot{q}'(\mathbf{x}, t)$ and $p'(t)$ are anti-phase ($\pi/2 < |\Delta\phi| < \pi$), energy is removed locally from the acoustic field (Fig. 1b-III)^{40,42}. The state of thermoacoustic instability arises when the aggregate energy added to the acoustic field from the entire spatial domain is greater than the net energy losses from the acoustic field⁴¹.

In synchronization theory, the conformist oscillators promote global synchrony, whereas the contrarian oscillators hinder the emergence of synchrony due to their opposing behavior²². The correlated in-phase dynamics adds energy to the acoustic field, whereas the correlated anti-phase dynamics removes energy from the acoustic field. Therefore, the influence of the correlated in-phase and the correlated anti-phase dynamics on the acoustic field is similar to the influence of conformist and contrarian oscillators on global synchrony. Using the cross-correlation measures, we classify the dynamics of $\dot{q}'(\mathbf{x}, t)$ and $p'(t)$ as uncorrelated (disordered), correlated in-phase (conformist), and correlated anti-phase (contrarian) dynamics. A state variable ($S(\mathbf{x}, t)$) is introduced to represent the dynamics at a spatial location, represented as $S(\mathbf{x}, t) = [S_{\text{conf}}, S_{\text{cont}}, S_{\text{dis}}]$ (refer equations 7-9 in *Materials and Methods*). Here, the subscript ‘conf’, ‘cont’, and ‘dis’ represent the conformist, contrarian, and disordered dynamics respectively.

Next, we define order parameters for each of these dynamics, for example, the order parameter for the conformist dynamics represents its fraction in the spatial domain, denoted as,

$$\rho_{\text{conf}}(t) = \frac{1}{L^2} \sum_{\mathbf{x}} S_{\text{conf}}(\mathbf{x}, t), \quad (2)$$

where, L^2 is the size of the spatial domain. In a similar manner, order parameters are defined for

the contrarian (ρ_{cont}) and the disordered dynamics as well (ρ_{dis}).

$$\rho_{\text{cont}}(t) = \frac{1}{L^2} \sum_{\mathbf{x}} S_{\text{cont}}(\mathbf{x}, t), \quad (3)$$

$$\rho_{\text{dis}}(t) = \frac{1}{L^2} \sum_{\mathbf{x}} S_{\text{dis}}(\mathbf{x}, t). \quad (4)$$

We study the variation of the order parameters for each of these dynamics for the smooth and abrupt transitions in a turbulent reactive flow system.

III. RESULTS

A. Significant presence of disordered dynamics in the spatial domain during the smooth transition

The spectrogram and the amplitude of the acoustic pressure oscillations (green color) during the smooth transition are shown in Fig. 2a, b respectively. As the control parameter, the Reynolds number (Re) is increased, a gradual rise in the amplitude of the acoustic pressure fluctuations is observed (Fig. 2b). The normalized acoustic pressure oscillations and the normalized heat release rate oscillations for different dynamical states during the smooth transition are shown in Fig. 2c. The global heat release rate fluctuations ($\dot{q}'_G(t)$) are determined by summing the distribution of the local heat release rate oscillations which are obtained from the chemiluminescence imaging, i.e., $\dot{q}'_G(t) = \sum_{\mathbf{x}} \dot{q}'(\mathbf{x}, t)$. Throughout this paper, the normalized variables are denoted with a subscript 'n', and the variables are normalized using their respective standard deviation values.

Initially ($Re = 1.66 \times 10^4$), we observe low-amplitude aperiodic acoustic pressure oscillations which have been identified as high-dimensional chaos (Fig. 2b-I and Fig. 2c-I)⁴³. During the state of chaos, $\dot{q}'_{Gn}(t)$ and $p'_n(t)$ exhibit desynchronized dynamics (Fig. 2c-I)⁴⁴. By increasing Re , we observe a smooth transition to a sustained, low-amplitude periodic oscillatory state, known as limit cycle oscillations (Fig. 2b-III and Fig. 2c-III). $\dot{q}'_{Gn}(t)$ and $p'_n(t)$ exhibit synchronized dynamics during the sustained periodic oscillatory state (Fig. 2c-III)⁴⁴. A state of intermittency where periodic oscillations appear amidst aperiodic oscillations is observed before the transition to the sustained periodic oscillatory state (Fig. 2c-II)¹. The transition to the state of sustained periodic oscillations in the acoustic pressure is indicated by the appearance of a narrow, bright, continuous band in its spectrogram (Fig. 2a). The frequency of these periodic oscillations is 199 Hz, corresponding to

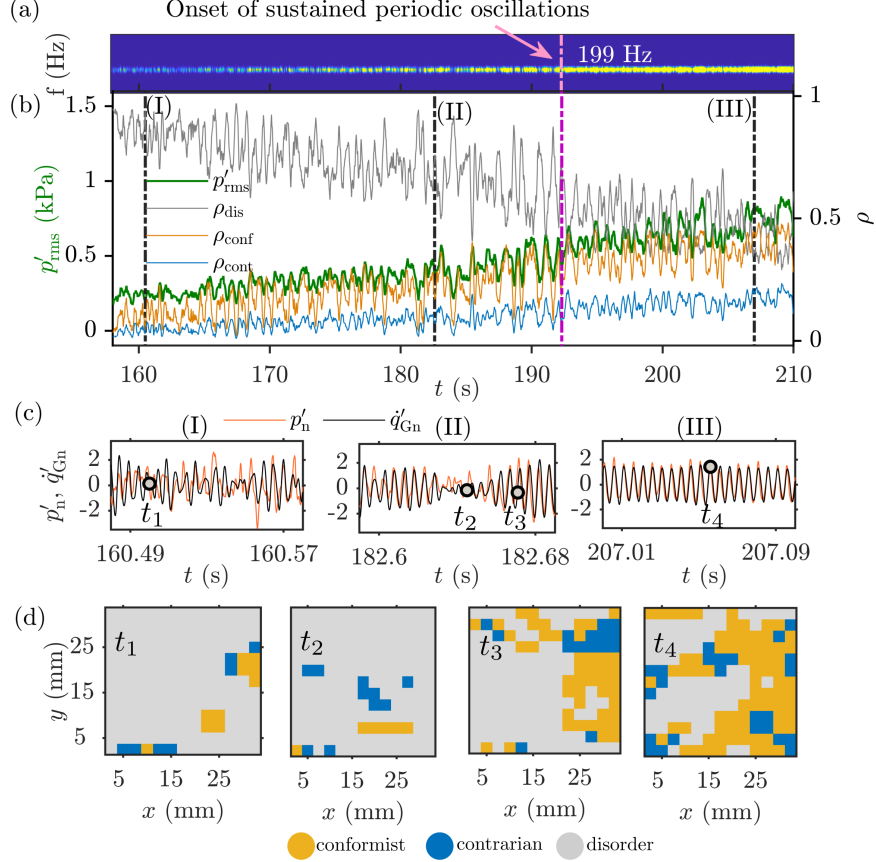


FIG. 2. (a) Spectrogram of the acoustic pressure oscillations, (b) the variation of the rms values of the acoustic pressure fluctuations (green), and the evolution of the order parameters for the conformist (orange), contrarian (blue), and disordered dynamics (gray) corresponding to the smooth transition. The rms values are calculated for a moving window of duration 0.5 s. The transition to the state of sustained periodic oscillations is evident in the spectrogram of the acoustic pressure oscillations and the rms values of the acoustic pressure oscillations gradually increase during this smooth transition. (c) The normalized $\dot{q}'_G(t)$ and the normalized $p'(t)$ for the state of (I) low-amplitude aperiodic fluctuations, (II) intermittency, and (III) periodic oscillations for the epochs represented with black dashed lines in (b). (d) The spatial distribution of conformist, contrarian, and disordered dynamics correspond to the epochs t_1 to t_4 in (c). During the smooth transition, we observe the dominance of conformist dynamics over contrarian dynamics. This smooth transition is accompanied by a significant presence of disordered dynamics in the spatial domain.

the fundamental longitudinal acoustic mode of the combustion chamber.

Figure 2d represents the spatial distribution of conformist (yellow), contrarian (blue), and disordered dynamics (grey) for four different epochs (labeled as t_1 to t_4 in Fig. 2c) across the smooth transition. During the chaotic and the aperiodic epoch of the state of intermittency, the disordered dynamics is dominant in the spatial domain along with a negligible fraction of conformist and contrarian dynamics (Fig. 2d- t_1 and Fig. 2d- t_2). However, during the periodic epoch of the state of intermittency, conformist and contrarian dynamics emerge in the spatial domain (Fig. 2d- t_3).

After the transition to the state of sustained periodic oscillations (Fig. 2b-III), we observe that the fraction of regions exhibiting the conformist dynamics is greater than the fraction of regions exhibiting the contrarian dynamics (Fig. 2d- t_4) along with a significant spatial extent of the disordered dynamics that neither add nor remove energy from the acoustic field (Fig. 2d- t_4). A greater fraction of conformist dynamics than contrarian dynamics ensures a continuous addition of energy to the acoustic field.

The variation of order parameters for the conformist (ρ_{conf}), contrarian (ρ_{cont}), and disordered (ρ_{dis}) dynamics across the smooth transition is shown in orange, blue, and grey colors respectively in Fig. 2b. During the smooth transition, we observe a gradual, monotonic increase of ρ_{conf} and ρ_{cont} from a very small value close to zero to values of 0.38 and 0.15 respectively at $t = 210$ s (Fig. 2b). Meanwhile, the disordered dynamics ρ_{dis} , gradually decreases from 1 to 0.47 (Fig. 2b). Therefore, we observe that the conformist dynamics dominate over the contrarian dynamics, along with a significant spatial extent of disordered dynamics during the smooth transition from chaos to order (Fig. 2b).

B. Disappearance of disordered dynamics from the spatial domain accompanying abrupt transitions

Further, we consider two different scenarios: (1) a smooth transition followed by an abrupt transition and (2) an abrupt transition depicted in Fig. 1c-II and Fig. 1c-III, respectively.

For the first scenario, the spectrogram and the amplitude of the acoustic pressure oscillations are shown in Fig. 3a, b. During this initial smooth transition, the amplitude of the acoustic pressure oscillations (green color line in Fig. 3b) gradually increases while we observe a transition from a low-amplitude aperiodic oscillatory state (Fig. 3b-I and Fig. 3c-I) to a low-amplitude periodic oscillatory state (Fig. 3b-III and Fig. 3c-III) through a state of intermittency (Fig. 3c-II). This transition from an aperiodic state to a state of sustained periodic oscillations is evident in the spectrogram of the acoustic pressure oscillations (Fig. 3a). Further, this smooth transition is followed by an abrupt transition to a high-amplitude periodic oscillatory state (Fig. 3c-IV).

During the low-amplitude aperiodic acoustic pressure oscillations, disordered dynamics dominate the spatial domain (Fig. 3c and Fig. 3d- t_1). We observe that the disordered dynamics are dominant during the aperiodic epoch of the state of intermittency as well (Fig. 3d- t_2). However, during the periodic epoch of the state of intermittency, the conformist and contrarian dynamics

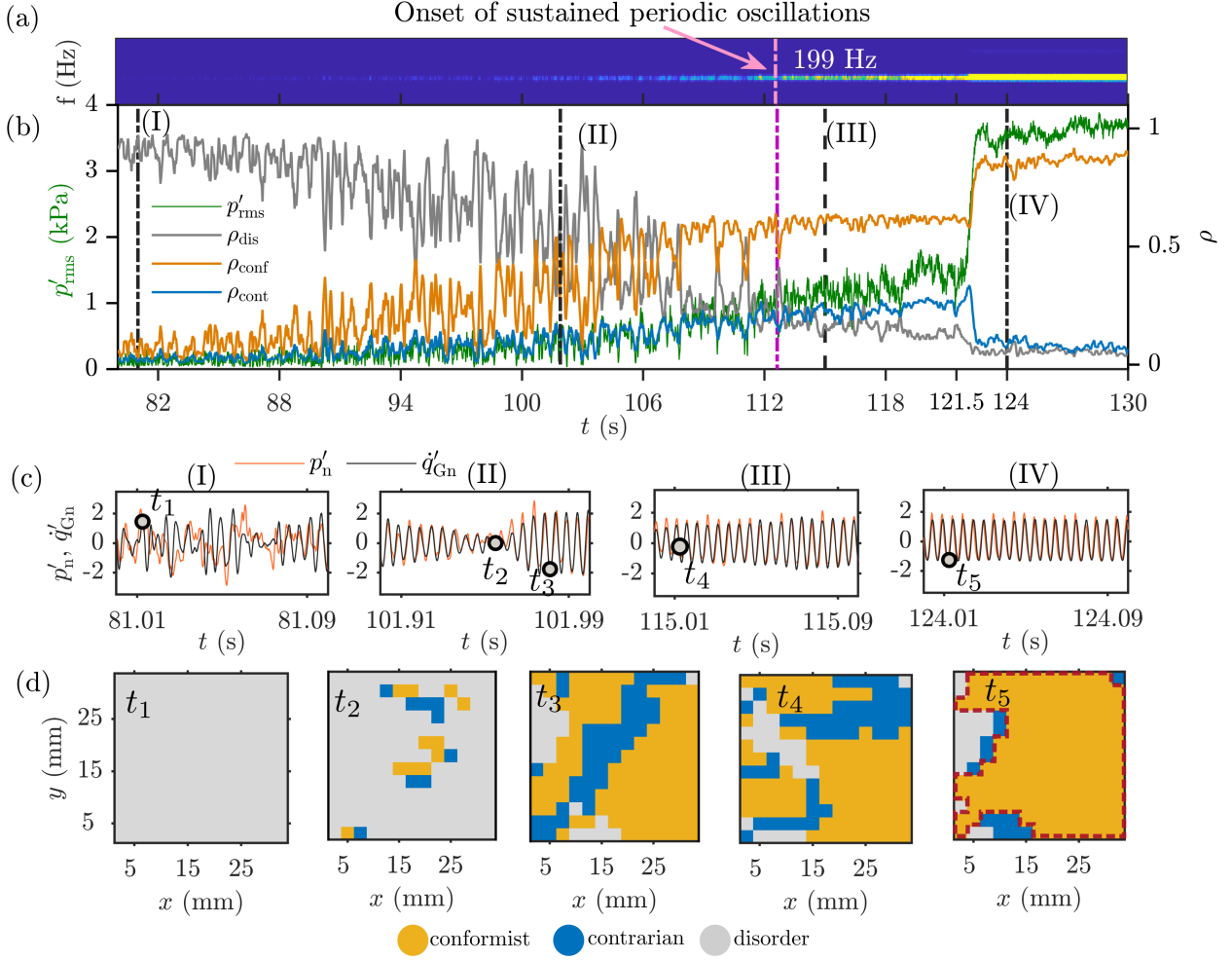


FIG. 3. (a) The spectrogram and (b) the variation of the rms values of $p'(t)$ for the smooth transition from a state of chaotic oscillations to a state of low-amplitude periodic oscillatory state followed by an abrupt transition to a high-amplitude periodic oscillatory state. (c) The normalized $q'_G(t)$ and the normalized $p'(t)$ for the state of (I) low-amplitude aperiodic oscillations, (II) intermittency, (III) low-amplitude periodic oscillatory state, (IV) high-amplitude periodic oscillatory state for the epochs marked with black dashed lines in (b). (d) The spatial distribution of conformist, contrarian, and disordered dynamics for the epochs labeled with t_1 to t_5 in (c). The evolution of the order parameters for the conformist, contrarian, and disordered dynamics during this transition is shown in (b). During the smooth transition, the conformist and contrarian dynamics emerge in the spatiotemporal domain. Further, an abrupt transition to a high-amplitude periodic oscillatory state is accompanied by an abrupt rise of ρ_{conf} and a transition to a state with minimal presence of disordered dynamics. A giant cluster exhibiting conformist dynamics, highlighted with a brown-dashed line in (d- t_5) emerges in the spatial domain accompanying the abrupt transition.

emerge in the spatial domain (Fig. 3d- t_3). During the low-amplitude periodic oscillatory state prior to the abrupt transition, we observe that medium-sized clusters of conformist dynamics are separated by clusters of contrarian and disordered dynamics (Fig. 3d- t_4). After the abrupt transition, we observe that the contrarian and disordered dynamics separating the medium-sized clusters

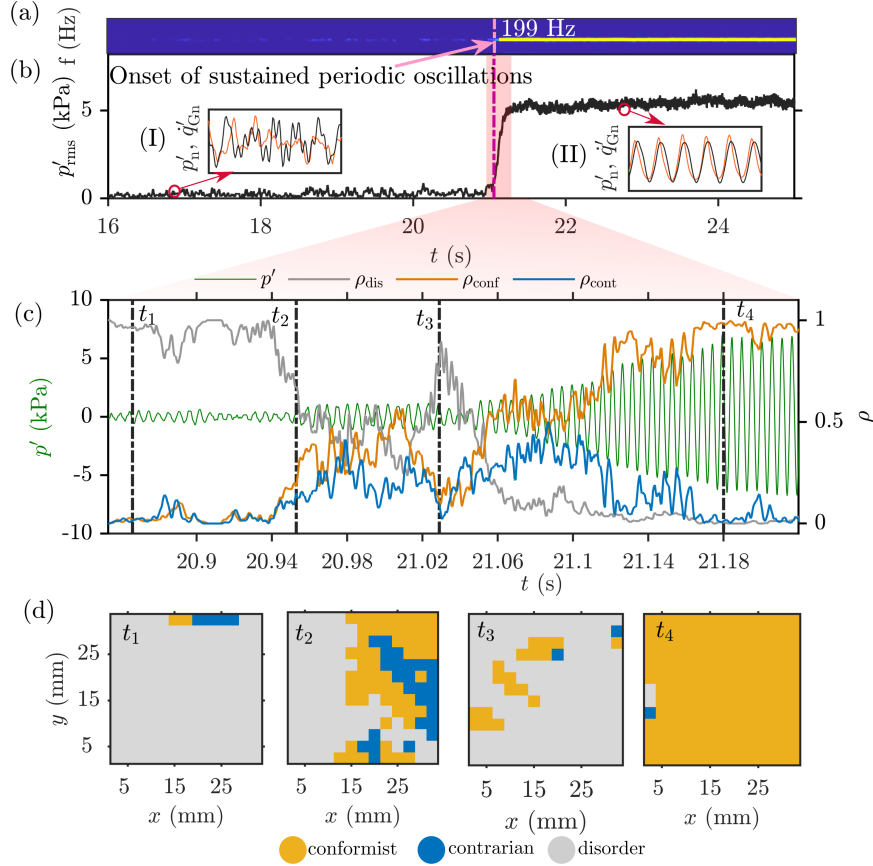


FIG. 4. (a) The spectrogram and (b) the variation of the rms values of $p'(t)$ for the abrupt transition from a state of chaotic fluctuations to a state of high-amplitude periodic oscillations. A small window of duration 0.5 s is considered for finding the rms of $p'(t)$. The abrupt appearance of sustained periodic oscillations is evident in the spectrogram. $p'_n(t)$ and $q'_{Gn}(t)$ corresponding to the state of chaotic and high-amplitude periodic oscillations are shown in (b-I), and (b-II) respectively. (c) The zoomed-in view of $p'(t)$ and the evolution of the order parameters within the red box in (b). (d) The spatial distribution of conformist, contrarian, and disordered dynamics for the epochs t_1 to t_4 in (c). We find that the conformist dynamics dominate the contrarian dynamics after the abrupt transition. Accompanying this abrupt transition, the system transitions to a state with minimal disordered dynamics in the spatial domain.

of conformist dynamics have disappeared, and a giant cluster of conformist dynamics that spans the entire spatial domain has emerged, which is highlighted with a brown-dashed line in Fig. 3d- t_5 .

The evolution of the order parameters (ρ_{conf} , ρ_{cont} , and ρ_{dis}) across the smooth transition followed by an abrupt transition is shown in Fig. 3b. During the low-amplitude aperiodic oscillations (until $t = 88$ s), the order parameters for both conformist and contrarian dynamics remain nearly zero ($\rho_{conf} \approx 0$ and $\rho_{cont} \approx 0$). During this state of aperiodic oscillations, the order parameter associated with disordered dynamics is close to one ($\rho_{dis} \approx 1$). The values of ρ_{conf} and ρ_{cont} increase from 0 to 0.59 and 0.20 respectively between $t = 88$ s and $t = 112$ s. Meanwhile, the

disordered dynamics, ρ_{dis} decreases from 1 to 0.21. Between the interval (from $t = 88$ s to $t = 112$ s), we observe large fluctuations in ρ_{conf} and ρ_{dis} due to the appearance of intermittent periodic oscillations (Fig. 3c-II). Furthermore, during the sustained low-amplitude periodic oscillatory state (between $t = 112.6$ s and $t = 121$ s), the values of ρ_{conf} and ρ_{cont} gradually increases to 0.63 and 0.27 respectively, meanwhile ρ_{dis} continues to decrease and reach a value of 0.1 at $t = 121$ s.

After $t = 121.5$ s, we observe an abrupt transition indicated by a steep rise in the amplitude of p' and an abrupt rise of ρ_{conf} (Fig. 3b). The abrupt rise in the amplitude of p' coincides with an initial increase of ρ_{cont} , but then ρ_{cont} decreases to a very small value during this abrupt transition (after $t = 121.5$ s in Fig. 3b). More importantly, we find that the system transitions to a state with minimal disordered dynamics accompanying this abrupt transition.

For the second scenario, as illustrated in Fig. 1c-III, we observe an abrupt transition from a state of low-amplitude aperiodic acoustic pressure oscillations (Fig. 4b-I) to a state of high-amplitude periodic oscillatory state (Fig. 4b-II). This abrupt transition is marked by the sudden appearance of a narrow, bright band in the spectrogram of the acoustic pressure oscillations indicated in Fig. 4a. To understand the dynamics during the abrupt transition, consider the zoomed-in view of the epoch highlighted with red color in Fig. 4b, which is shown in Fig. 4c.

The evolution of order parameters and the spatial distribution of the conformist, contrarian, and disordered dynamics during the abrupt transition is shown in Fig. 4c and Fig. 4d, respectively. During the low-amplitude acoustic pressure fluctuations, the spatial regions exhibiting the disordered dynamics are very high as compared to the conformist and contrarian dynamics (Fig. 4d- t_1). We observe the emergence of sustained periodic acoustic pressure oscillations after $t = 20.94$ s onwards (Fig. 4c). The amplitude of these periodic oscillations initially increases from $t = 20.94$ s to $t = 20.98$ s, while ρ_{conf} and ρ_{cont} increase from 0 to 0.36 and 0.26 respectively. During this epoch (from $t = 20.94$ s to $t = 20.98$ s), ρ_{dis} decreases from 1 to 0.38. Further, the amplitude of the acoustic pressure oscillations does not grow monotonically, it decreases later (from $t = 21.02$ s to $t = 21.04$ s). Therefore we observe a non-monotonic variation of ρ_{conf} , ρ_{cont} and ρ_{dis} between $t = 21.02$ s and $t = 21.04$ s (Fig. 4c). ρ_{dis} increases first and then decreases whereas ρ_{conf} and ρ_{cont} decreases first and then increases. Further, ρ_{dis} continues to decrease and reach a small value of 0.15 around $t = 21.06$ s. Eventually, after $t = 21.1$ s, we observe an abrupt transition indicated by a rapid rise of $p'(t)$ and ρ_{conf} (Fig. 4c). Accompanying this abrupt transition, we find that the system transitions to a state with minimal disordered dynamics (Fig. 4c and Fig. 4d- t_4).

IV. DISCUSSIONS

In a reactive flow system operating in turbulent conditions, we observe (1) a smooth transition, (2) a smooth transition followed by an abrupt transition, and (3) an abrupt transition from chaos to order for different experimental conditions (Fig. 1c). We observe the dominance of conformist dynamics over contrarian dynamics during all three transitions we have discussed. The dominance of conformist dynamics maintains a flux of energy to the acoustic field during the state of sustained periodic oscillations. Notably, the evolution of disordered dynamics during the smooth and abrupt transitions differ. During the smooth transition (Fig. 1c-I), we observe a significant spatial extent of disordered dynamics (Fig. 2b). Bhavi *et al.*⁴ reveals that turbulence intensity, in comparison to the amplitude of the limit cycle oscillations, smoothens the abrupt transition to the state of limit cycle oscillations. In the case of a smooth transition followed by an abrupt transition (Fig. 1c-II), during the initial smooth transition, the disordered dynamics become minimal and continue to decrease, followed by an abrupt transition accompanied by the disappearance of disordered dynamics (Fig. 3b). The abrupt transition illustrated in Fig. 1c-III is accompanied by the disappearance of disordered dynamics (Fig. 4c). In summary, we discover that the spatial extent of disordered dynamics plays a crucial role in deciding the nature of the transition. During the smooth transition, we observe a significant presence of disordered dynamics. In contrast, the abrupt transition is accompanied by the disappearance of disordered dynamics from the spatial domain.

In this paper, we have studied smooth and abrupt transitions from chaos to order by classifying various dynamics between the acoustic pressure and the heat release rate oscillations based on their influence on the acoustic energy of the system. Our methodology is inspired and based on the principles of synergetics and phase transition, wherein order parameters are defined for various plausible configurations to study the emergent behavior in complex systems⁴⁵. Our study provides insights on the role of disordered dynamics on the occurrence of smooth and abrupt transitions in a real-world complex system.

V. MATERIALS AND METHODS

A. Experimental setup

We performed experiments in a reactive flow system operating in turbulent conditions (Fig. 1a). Our experimental setup consists of a settling chamber, mixing pipe, swirler, and combustion chamber of 800 mm in length. Air is first passed through a moisture separator and then flows into the settling chamber. We use liquified petroleum gas, composed of 40% C_3H_8 and 60% C_4H_{10} by volume, as fuel. The fuel is supplied into the mixing pipe through a central shaft with four radial injection holes, each with a diameter of 1.7 mm. These injection holes are located 100 mm upstream of the exit plane of the mixing pipe. A swirler is used to introduce radial momentum to the reactants flowing axially inside the mixing pipe. The swirler consists of eight fixed vanes of 1 mm thickness and 30 mm length. The fixed vane has a bent of 40° about the axial direction of the combustion chamber. The swirler has a central body with a diameter of 16 mm and a length of 30 mm. The swirler is positioned in such a way that the downstream end of the swirler is aligned with the exit plane of the mixing pipe. The partially premixed air and fuel (reactants) inside the mixing pipe flow into the combustion chamber through a backward-facing step. The outlet of the combustion chamber is connected to a decoupler of size 1000 mm \times 500 mm \times 500 mm, which isolates the system from ambient fluctuations.

The air and fuel flow rates are controlled by mass flow controllers (Alicat scientific MCR series). The mass flow controllers have an uncertainty of $\pm 0.8\%$ of the measured reading + 0.2% of full-scale reading. The Reynolds number (Re) is defined as $\rho \bar{v} D / \mu$, where μ and ρ are the dynamic viscosity and density of the reactants calculated by considering the chemical composition of the reactants⁴⁶, D is the diameter of the swirler, and \bar{v} is the average velocity of the reactants at the backward-facing step of the combustion chamber.

We conduct experiments by varying the flow rate of air from 7.76 g/s to 12.66 g/s for three different rates of 0.02, 0.03, and 0.2 g/s². The fuel flow rate is kept constant at 0.75 g/s during these experiments. This leads to the variation in the Reynolds number from 1.60×10^4 to 2.50×10^4 for three different rates: (1) $dRe/dt = 340$ 1/s, (2) $dRe/dt = 60$ 1/s and (3) $dRe/dt = 38$ 1/s. Corresponding to these three different rates, we observe a smooth transition, a smooth transition followed by an abrupt transition, and an abrupt transition.

A piezoelectric pressure transducer (PCB103B02) is flush mounted to the wall of the combus-

tion chamber at 120 mm downstream of the backward-facing step of the combustion chamber is used to measure the acoustic pressure oscillations inside the combustion chamber. The pressure transducer has an uncertainty of ± 0.15 Pa and a sensitivity of 217.50 mV/kPa. The electrical signals from the piezoelectric pressure transducer were reordered at a sampling rate of 4000 Hz using a 16-bit analog-to-digital data acquisition system (NI-6143). The CH* chemiluminescence intensities represent the heat release rate fluctuations^{47,48}. A high-frame-rate camera (Phantom v12.1) with a Carl-Zeiss lens of 100 mm focal length, outfitted with a CH* filter, is used to record the chemiluminescence images. The outfitted CH* filter is characterized by a narrow bandwidth centered at 435 nm and has a full width at half maximum of 10 nm. The images were recorded at a sampling rate of 2000 Hz, simultaneously with the piezoelectric pressure transducer. The recorded images have a resolution of 512×400 pixels.

B. Classifying the correlated dynamics

In this section, we classify different correlated dynamics of the acoustic pressure fluctuations and the heat release rate fluctuations as shown in Fig. 1b. The region where the flame is present is very small relative to the acoustic wavelength. Therefore, the acoustic pressure can be considered to be uniform within the reaction zone². We consider a linear correlation measure since the acoustic driving in reactive flow systems is proportional to the linear cross-correlation between the acoustic pressure fluctuations and the heat release rate fluctuations^{40,41,49}. The cross-correlation between $\dot{q}'_n(\mathbf{x}, t)$ and $p'_n(t)$ for different time delay values are defined as

$$\mathcal{R}(\mathbf{x}, t, \tau_i) = \int_t^{t+W} p'_n(t_1) \dot{q}'_n(\mathbf{x}, t_1 + \tau_i) dt_1. \quad (5)$$

The cross-correlation values, \mathcal{R} , are calculated over a short duration (W) of $4T$, with T representing the time period of the fundamental longitudinal mode of the acoustic oscillations. Our results are consistent for different short time window values (*Supporting Information* Fig. 6). \mathcal{R} is calculated for distinct time delay values (τ_i) from $-T/2$ to $+T/2$.

For the uncorrelated fluctuations in $\dot{q}'(\mathbf{x}, t)$ and $p'(t)$, $\mathcal{R}(\mathbf{x}, t)$ values remain small (Fig. 5b, d), regardless of the time delay values. In contrast, for the correlated fluctuations, a high correlation value ($\mathcal{R}(\mathbf{x}, t)$) close to one is observed for a time lag value equivalent to the phase difference

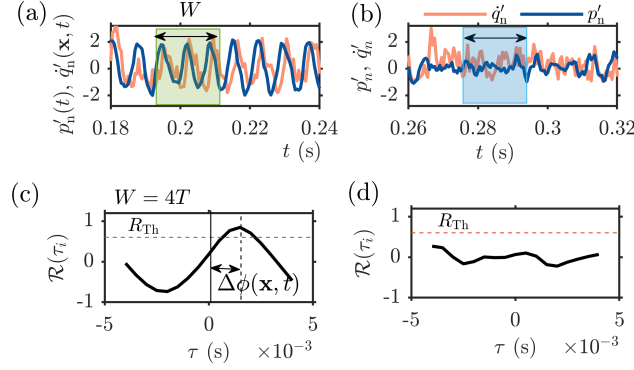


FIG. 5. The normalized heat release rate oscillations (orange color) from a spatial location and the normalized acoustic pressure oscillations (blue color) for the state of (a) periodic and (b) aperiodic oscillations. (c, d) Cross-correlation values (\mathcal{R}) for a duration of $W = 4T$ between \dot{q}'_n and p'_n for various lag values (τ_i) for the epochs highlighted in (a, b). The orange dotted line is the threshold value for classifying the uncorrelated and correlated dynamics. For the uncorrelated dynamics, as shown in (d), the values of \mathcal{R} remain very small for all τ values. However, for the correlated dynamics, $\mathcal{R} \approx 1$, when τ_i is equal to $\Delta\phi(\mathbf{x}, t)$. Using this methodology, we distinguish the uncorrelated and the correlated dynamics.

between $p'(t)$ and $\dot{q}'(\mathbf{x}, t)$ (Fig. 5a, c). Finally, the maximum value among the correlation values for different time lag values is selected, expressed as

$$R_{\max}(\mathbf{x}, t) = \max \text{ for all } \tau_i \{ \mathcal{R}(\mathbf{x}, t, \tau_i) \} = \mathcal{R}(\mathbf{x}, t, \Delta\phi(\mathbf{x}, t)), \quad (6)$$

where $\Delta\phi(\mathbf{x}, t)$ represents the phase difference between the variables, $\dot{q}'_n(\mathbf{x}, t)$ and $p'_n(t)$. By selecting an appropriate threshold for R_{\max} , we can identify the uncorrelated and correlated dynamics in the spatiotemporal domain as illustrated in Fig. 5. The threshold value for the R_{\max} values is 0.6 for the present study. We have shown that our results qualitatively remain the same for a range of threshold values (refer to *Supporting Information*, Fig. 7 for more details). The correlated dynamics with a time-shift value $|\Delta\phi(\mathbf{x}, t)| \leq \pi/2$ are in-phase correlated dynamics (conformist) and correlated dynamics with $\pi/2 < |\Delta\phi(\mathbf{x}, t)| < \pi$ are anti-phase correlated dynamics (contrarian).

Having defined different corrected dynamics, a state variable, $S(\mathbf{x}, t) = [S_{\text{conf}}, S_{\text{cont}}, S_{\text{dis}}]$, is introduced to represent these correlated dynamics. Here, the subscript ‘conf’, ‘cont’, and ‘dis’ represent the conformist, contrarian, and disordered dynamics, respectively. The state variable is

defined as,

$$S_{\text{conf}}(\mathbf{x}, t) = \begin{cases} 1 & \text{if } R_{\text{max}}(\mathbf{x}, t) \geq R_{\text{Th}} \text{ and } |\Delta\phi(\mathbf{x}, t)| \leq \pi/2, \\ 0 & \text{else.} \end{cases} \quad (7)$$

$$S_{\text{cont}}(\mathbf{x}, t) = \begin{cases} 1 & \text{if } R_{\text{max}}(\mathbf{x}, t) \geq R_{\text{Th}} \text{ and } \pi/2 < |\Delta\phi(\mathbf{x}, t)| < \pi, \\ 0 & \text{else.} \end{cases} \quad (8)$$

$$S_{\text{dis}}(\mathbf{x}, t) = \begin{cases} 1 & \text{if } R_{\text{max}}(\mathbf{x}, t) < R_{\text{Th}}, \\ 0 & \text{else.} \end{cases} \quad (9)$$

ACKNOWLEDGMENTS

We acknowledge Mrs. Shruti Tandon, Mr. Praveen Kumar, Mr. Ramesh S Bhavi, and Mr. Rohit R for their suggestions and feedback. We acknowledge Mr. P. R. Midhun, Mr. S. Anand, Mr. S. Thilagaraj, Mrs. G. Sudha and Dr. M. Ragunathan for their help during the experiments. RIS wishes to express his gratitude to the Department of Science and Technology and Ministry of Human Resource Development, Government of India for providing financial support for our research work under Grant No. JCB/2018/000034/SSC (JC Bose Fellowship).

REFERENCES

- ¹V. Nair, G. Thampi, and R. I. Sujith, “Intermittency route to thermoacoustic instability in turbulent combustors,” *Journal of Fluid Mechanics* **756**, 470–487 (2014).
- ²S. Sudarsanan, A. Roy, I. Pavithran, S. Tandon, and R. I. Sujith, “Emergence of order from chaos through a continuous phase transition in a turbulent reactive flow system,” *Phys. Rev. E* **109**, 064214 (2024).
- ³S. Singh, A. Roy, K. V. Reeja, A. Nair, S. Chaudhuri, and R. I. Sujith, “Intermittency, secondary bifurcation and mixed-mode oscillations in a swirl-stabilized annular combustor: Experiments and modeling,” *Journal of Engineering for Gas Turbines and Power* **143**, 051028 (2021).
- ⁴R. S. Bhavi, I. Pavithran, A. Roy, and R. I. Sujith, “Abrupt transitions in turbulent thermoacoustic systems,” *Journal of Sound and Vibration* **547**, 117478 (2023).
- ⁵E. H. Van Nes, B. M. S. Arani, A. Staal, B. van der Bolt, B. M. Flores, S. Bathiany, and

- M. Scheffer, “What do you mean, ‘tipping point’?” *Trends in Ecology & Evolution* **31**, 902–904 (2016).
- ⁶R. B. Yaffe, P. Borger, P. Megevand, D. M. Groppe, M. A. Kramer, C. J. Chu, S. Santaniello, C. Meisel, A. D. Mehta, and S. V. Sarma, “Physiology of functional and effective networks in epilepsy,” *Clinical Neurophysiology* **126**, 227–236 (2015).
- ⁷S. Boccaletti, J. Almendral, S. Guan, I. Leyva, Z. Liu, I. Sendiña-Nadal, Z. Wang, and Y. Zou, “Explosive transitions in complex networks’ structure and dynamics: Percolation and synchronization,” *Physics Reports* **660**, 1–94 (2016).
- ⁸R. M. D’Souza, J. Gómez-Gardenes, J. Nagler, and A. Arenas, “Explosive phenomena in complex networks,” *Advances in Physics* **68**, 123–223 (2019).
- ⁹L. Arola-Fernández, S. Faci-Lázaro, P. S. Skardal, E. C. Boghiu, J. Gómez-Gardeñes, and A. Arenas, “Emergence of explosive synchronization bombs in networks of oscillators,” *Communications Physics* **5**, 264 (2022).
- ¹⁰D. Pazó, “Thermodynamic limit of the first-order phase transition in the kuramoto model,” *Phys. Rev. E* **72**, 046211 (2005).
- ¹¹J. Gómez-Gardenes, S. Gómez, A. Arenas, and Y. Moreno, “Explosive synchronization transitions in scale-free networks,” *Physical Review Letters* **106**, 128701 (2011).
- ¹²I. Leyva, A. Navas, I. Sendiña-Nadal, J. Almendral, J. Buldú, M. Zanin, D. Papo, and S. Boccaletti, “Explosive transitions to synchronization in networks of phase oscillators,” *Scientific Reports* **3**, 1281 (2013).
- ¹³P. S. Skardal and A. Arenas, “Higher order interactions in complex networks of phase oscillators promote abrupt synchronization switching,” *Communications Physics* **3**, 218 (2020).
- ¹⁴A. P. Millán, J. J. Torres, and G. Bianconi, “Explosive higher-order Kuramoto dynamics on simplicial complexes,” *Physical Review Letters* **124**, 218301 (2020).
- ¹⁵S. Jalan, V. Rathore, A. D. Kachhvah, and A. Yadav, “Inhibition-induced explosive synchronization in multiplex networks,” *Physical Review E* **99**, 062305 (2019).
- ¹⁶X. Zhang, S. Guan, Y. Zou, X. Chen, and Z. Liu, “Suppressing explosive synchronization by contrarians,” *Europhysics Letters* **113**, 28005 (2016).
- ¹⁷V. Rathore, A. Suman, and S. Jalan, “Synchronization onset for contrarians with higher-order interactions in multilayer systems,” *Chaos: An Interdisciplinary Journal of Nonlinear Science* **33** (2023).
- ¹⁸J. Soriano, M. Rodríguez Martínez, T. Tlusty, and E. Moses, “Development of input connections

- in neural cultures,” *Proceedings of the National Academy of Sciences* **105**, 13758–13763 (2008).
- ¹⁹J. Myung, S. Hong, D. DeWoskin, E. De Schutter, D. B. Forger, and T. Takumi, “Gaba-mediated repulsive coupling between circadian clock neurons in the SCN encodes seasonal time,” *Proceedings of the National Academy of Sciences* **112**, E3920–E3929 (2015).
- ²⁰S. D. Yi, S. K. Baek, C.-P. Zhu, and B. J. Kim, “Phase transition in a coevolving network of conformist and contrarian voters,” *Phys. Rev. E* **87**, 012806 (2013).
- ²¹A. Girón, H. Saiz, F. S. Bacelar, R. F. Andrade, and J. Gómez-Gardenes, “Synchronization unveils the organization of ecological networks with positive and negative interactions,” *Chaos: An Interdisciplinary Journal of Nonlinear Science* **26** (2016).
- ²²H. Hong and S. H. Strogatz, “Kuramoto model of coupled oscillators with positive and negative coupling parameters: An example of conformist and contrarian oscillators,” *Physical Review Letters* **106**, 054102 (2011).
- ²³P. Kumar, D. K. Verma, P. Parmananda, and S. Boccaletti, “Experimental evidence of explosive synchronization in mercury beating-heart oscillators,” *Physical Review E* **91**, 062909 (2015).
- ²⁴S. Mahler, A. A. Friesem, and N. Davidson, “Experimental demonstration of crowd synchrony and first-order transition with lasers,” *Physical Review Research* **2**, 043220 (2020).
- ²⁵A. F. Taylor, M. R. Tinsley, F. Wang, Z. Huang, and K. Showalter, “Dynamical quorum sensing and synchronization in large populations of chemical oscillators,” *Science* **323**, 614–617 (2009).
- ²⁶I. Leyva, R. Sevilla-Escoboza, J. Buldú, I. Sendiña-Nadal, J. Gómez-Gardenes, A. Arenas, Y. Moreno, S. Gómez, R. Jaimes-Reategui, and S. Boccaletti, “Explosive first-order transition to synchrony in networked chaotic oscillators,” *Physical Review Letters* **108**, 168702 (2012).
- ²⁷D. Călugăru, J. F. Tetz, E. A. Martens, and H. Engel, “First-order synchronization transition in a large population of strongly coupled relaxation oscillators,” *Science Advances* **6**, eabb2637 (2020).
- ²⁸S. B. Pope, “Turbulent flows,” *Measurement Science and Technology* **12**, 2020–2021 (2001).
- ²⁹V. Nair and R. I. Sujith, “Multifractality in combustion noise: predicting an impending combustion instability,” *Journal of Fluid Mechanics* **747**, 635–655 (2014).
- ³⁰R. I. Sujith and V. R. Unni, “Complex system approach to investigate and mitigate thermoacoustic instability in turbulent combustors,” *Physics of Fluids* **32**, 061401 (2020).
- ³¹M. P. Juniper and R. I. Sujith, “Sensitivity and nonlinearity of thermoacoustic oscillations,” *Annual Review of Fluid Mechanics* **50**, 661–689 (2018).
- ³²R. Biggs, “*Rocketdyne-F-1 Saturn V first stage engine*” in *Remembering the Giants: Apollo*

- Rocket Propulsion Development*, edited by S. C. Fisher and S. A. Rahman (NASA, 2009) pp. 15–26.
- ³³T. C. Lieuwen and V. Yang, *Combustion instabilities in gas turbine engines: operational experience, fundamental mechanisms, and modeling* (American Institute of Aeronautics and Astronautics, 2005).
- ³⁴P. Kriesels, M. Peters, A. Hirschberg, A. Wijnands, A. Iafrati, G. Riccardi, R. Piva, and J. Bruggeman, “High amplitude vortex-induced pulsations in a gas transport system,” *Journal of Sound and Vibration* **184**, 343–368 (1995).
- ³⁵D. Green and W. G. Unruh, “The failure of the Tacoma bridge: A physical model,” *American Journal of Physics* **74**, 706–716 (2006).
- ³⁶I. Pavithran, V. R. Unni, A. J. Varghese, R. I. Sujith, A. Saha, N. Marwan, and J. Kurths, “Universality in the emergence of oscillatory instabilities in turbulent flows,” *Europhysics Letters* **129**, 24004 (2020).
- ³⁷I. Pavithran, V. R. Unni, A. J. Varghese, D. Premraj, R. I. Sujith, C. Vijayan, A. Saha, N. Marwan, and J. Kurths, “Universality in spectral condensation,” *Scientific Reports* **10**, 17405 (2020).
- ³⁸A. Krishnan, R. I. Sujith, N. Marwan, and J. Kurths, “On the emergence of large clusters of acoustic power sources at the onset of thermoacoustic instability in a turbulent combustor,” *Journal of Fluid Mechanics* **874**, 455–482 (2019).
- ³⁹A. Joseph, I. Pavithran, and R. I. Sujith, “Explosive synchronization in a turbulent reactive flow system,” *Chaos: An Interdisciplinary Journal of Nonlinear Science* **34** (2024).
- ⁴⁰L. Rayleigh, “The explanation of certain acoustical phenomena,” *Nature* **18**, 319–321 (1878).
- ⁴¹T. Poinso and D. Veynante, *Theoretical and numerical combustion* (RT Edwards, Inc., 2005).
- ⁴²J. Samaniego, B. Yip, T. Poinso, and S. Candel, “Low-frequency combustion instability mechanisms in a side-dump combustor,” *Combustion and Flame* **94**, 363–380 (1993).
- ⁴³J. Tony, E. A. Gopalakrishnan, E. Sreelekha, and R. I. Sujith, “Detecting deterministic nature of pressure measurements from a turbulent combustor,” *Physical Review E* **92**, 062902 (2015).
- ⁴⁴S. A. Pawar, A. Seshadri, V. R. Unni, and R. I. Sujith, “Thermoacoustic instability as mutual synchronization between the acoustic field of the confinement and turbulent reactive flow,” *Journal of Fluid Mechanics* **827**, 664–693 (2017).
- ⁴⁵H. Haken, “Synergetics,” *Physics Bulletin* **28**, 412 (1977).
- ⁴⁶R. B. Bird, W. E. Stewart, E. N. Lightfoot, and R. E. Meredith, “Transport phenomena,” *Journal of The Electrochemical Society* **108**, 78C (1961).

- ⁴⁷Y. Hardalupas and M. Orain, “Local measurements of the time-dependent heat release rate and equivalence ratio using chemiluminescent emission from a flame,” *Combustion and Flame* **139**, 188–207 (2004).
- ⁴⁸F. Guethe, D. Guyot, G. Singla, N. Noiray, and B. Schuermans, “Chemiluminescence as diagnostic tool in the development of gas turbines,” *Applied Physics B* **107**, 619–636 (2012).
- ⁴⁹K. C. Schadow and E. Gutmark, “Combustion instability related to vortex shedding in dump combustors and their passive control,” *Progress in Energy and Combustion Science* **18**, 117–132 (1992).

VI. SUPPORTING INFORMATION

A. Dependence of the window size of the time series

In this section, we discuss the effect of choosing different window sizes for classifying the dynamics between the heat release rate and the acoustic pressure oscillations. We have selected window sizes ranging from $W = 3T$ to $W = 6T$, where T is the time period of the dominant mode of the acoustic pressure oscillations. We have calculated the order parameters for the conformist, contrarian, and disordered dynamics for these different window sizes. For all the window sizes we have considered, we observe a significant presence of disordered dynamics for the smooth transition. Further, accompanying the abrupt transition, the disordered dynamics have disappeared from the spatiotemporal domain. Therefore, for the different window sizes, the qualitative variation of the order parameters remains the same during (1) a smooth transition, (2) a smooth transition followed by an abrupt transition, and (3) an abrupt transition (Fig. 6).

B. Dependence of the threshold value

Here, we discuss the effect of selecting a different threshold value on our results. For this purpose, we have identified the correlated and the uncorrelated dynamics for different threshold values (R_{th}) of 0.55, 0.6, 0.65 and 0.7. The order parameters are then calculated for the conformist, contrarian, and disordered dynamics for different threshold values. We observe that, for all the threshold values we considered, the evolution of the order parameters, ρ_{conf} , ρ_{cont} , and ρ_{dis} remain qualitatively the same (Fig. 6) for smooth and abrupt transitions.

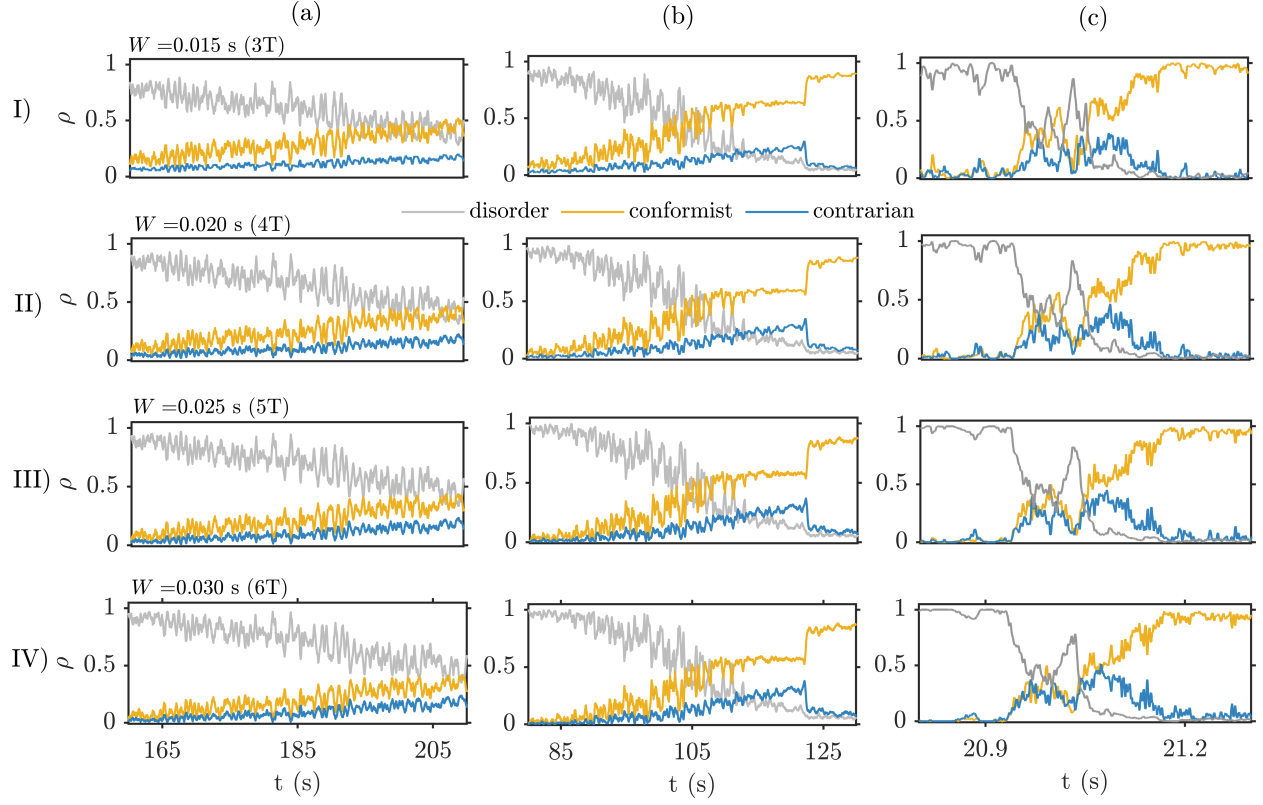


FIG. 6. a-e, The evolution of the order parameters for conformist, contrarian, and disordered dynamics for different window sizes of $W = 3T, 4T, 5T$, and $6T$. Our results qualitatively remain the same for different window sizes considered.

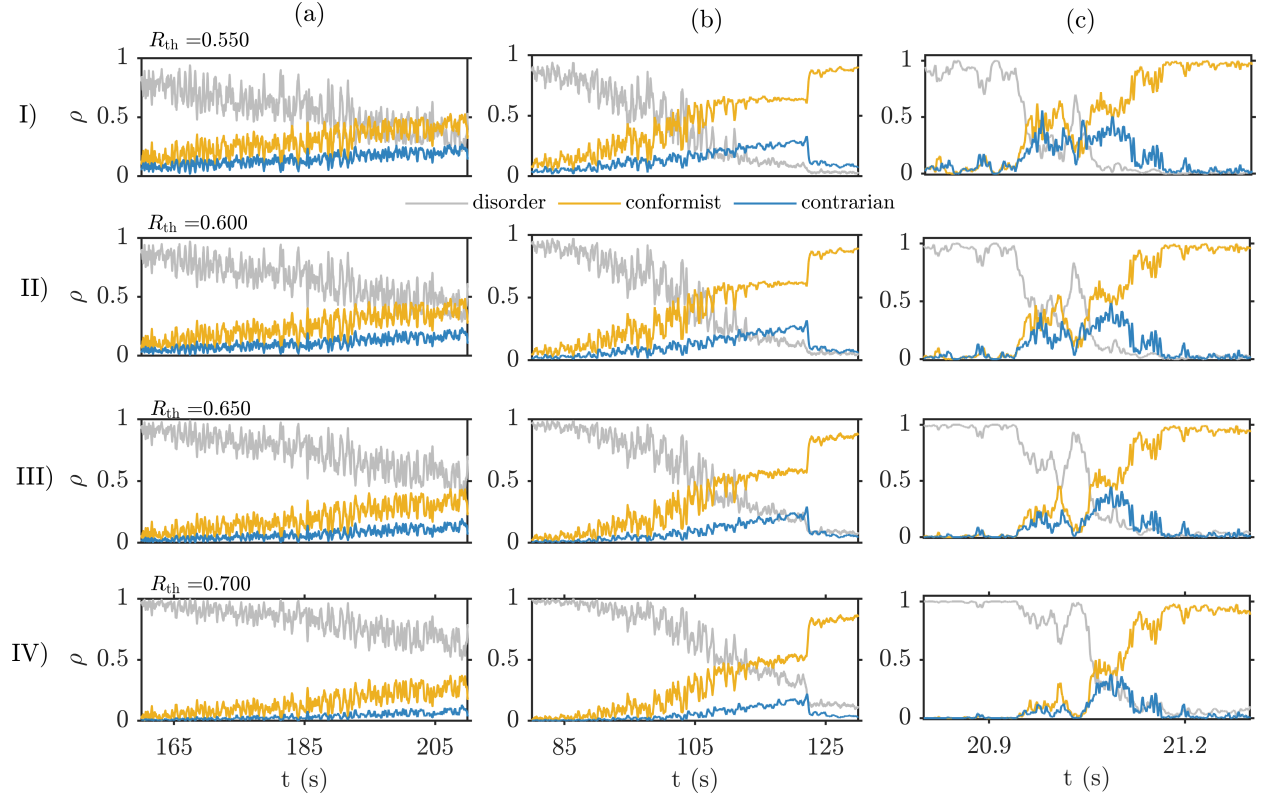


FIG. 7. a-c, The evolution of the order parameters for the conformist, contrarian, and disordered dynamics for different values of $R_{th} = 0.55, 0.6, 0.65$, and 0.7 . The evolution of order parameters remains qualitatively the same across (1) a smooth transition, (2) a smooth transition followed by an abrupt transition, and (3) an abrupt transition for a range of threshold values between 0.55 and 0.7 .